nature communications

Article

https://doi.org/10.1038/s41467-024-55013-3

Neuronal PRDX-2-Mediated ROS Signaling Regulates Food Digestion via peripheral UPR^{mt} Activation

Received: 16 February 2024

Accepted: 25 November 2024

Published online: 04 December 2024

Check for updates

Yating Liu[1,2], Qian Li[1,2], Guojing Tian[1], Xinyi Zhou[1], Panpan Chen[1], Bo Chen[1], Zhao Shan[1] ✉ & Bin Qi[1] ✉

All organisms depend on food digestion for survival, yet the brain-gut signaling mechanisms that regulate this process are not fully understood. Here, using an established *C. elegans* digestion model, we uncover a pathway in which neuronal ROS (free radicals) signal the intestine to suppress digestion. Genetic screening reveals that reducing genes responsible for maintaining ROS balance increases free radicals and decreases digestion. PRDX-2 knockout in olfactory neurons (AWC) elevates ROS and reduces digestive capacity, mediated by the neuropeptide NLP-1 and activation of the mitochondrial unfolded protein response (UPR^{mt}) in the intestine. Additionally, overexpressing *nlp-1* or ablating AWC neurons both trigger UPR^{mt} and inhibit digestion. These findings reveal a brain-gut connection in which neuronal PRDX-2-mediated ROS signaling modulates food digestion, highlighting a critical role of free radicals in shutting down digestion to alleviate stress and reduce food consumption.

Food is an essential source of nourishment for all living beings, supplying the energy required for growth and vital cellular activities. The digestion of food, a complex and health-critical process, involves the conversion of consumed food into nutrients that the body can utilize for growth, cellular upkeep, and energy production. This process is controlled by both neural and hormonal systems. Sensory neurons of the vagus nerve within the gastrointestinal tract oversee the stomach's volume and the intestinal contents, thereby managing digestive physiology[1]. Upon nutrient consumption, enteroendocrine cells are activated, leading to the release of gut hormones such as serotonin, glucagon-like peptide 1 (GLP1), cholecystokinin (CCK), peptide YY, among others[2]. These gut hormones have diverse roles in digestion, including the secretion of digestive juices, slowing down stomach emptying, regulating energy equilibrium, and maintaining blood glucose levels.

The food digestive system is a key area of interest for researchers and professionals in diverse fields such as nutrition, toxicology, pharmacology, and microbiology. However, the intricate and multi-stage nature of human digestion presents considerable challenges for research. These challenges are amplified by the substantial costs associated with such studies and the ethical dilemmas that emerge, particularly when the research involves potentially harmful entities such as xenobiotics or pathogenic microorganisms[3]. In our prior research, we utilized *C. elegans* as an animal model and discovered that *C. elegans* cannot digest non-edible food, such as *Staphylococcus saprophyticus*[4]. Interestingly, this non-edible food can be digested and utilized as a food source if heat-killed *Escherichia coli* is present, or by inhibiting the innate immune pathway, PMK-1[5]. Consequently, the non-edible bacteria (*Staphylococcus saprophyticus*)-worm culture system serves as an efficient and cost-effective animal model to investigate the molecular mechanism underlying food digestion in animals[6]. Using this digestive system, we found that signals such as outer membrane proteins[5] and peptidoglycan[7] from heat-killed *E. coli* activate the worm's food digestive system, enabling them to digest non-edible food SS to support growth. We also discovered that activation of

[1]Southwest United Graduate School, Yunnan Key Laboratory of Cell Metabolism and Diseases, State Key Laboratory of Conservation and Utilization of Bioresources in Yunnan Center for Life Sciences, School of Life Sciences, Yunnan University, Kunming, China. [2]These authors contributed equally: Yating Liu, Qian Li. ✉e-mail: shanzhaolab@163.com; qb@ynu.edu.cn

UPR^{mt} inhibits food digestion. However, it remains unclear whether brain-gut signaling regulates food digestion through regulating intestinal UPR^{mt}.

Reactive Oxygen Species (ROS) are recognized to participate in various signaling pathways in several peripheral organs, including the hypothalamus[8]. In the hypothalamus, ROS regulate food consumption and metabolism by influencing different types of neurons, such as proopiomelanocortin (POMC) and agouti-related protein (AgRP)/neuropeptide Y (NPY) neurons[9]. When in a fed state, the effects of glucose, lipids, insulin, and leptin lead to the release of ROS in both neuron types. This transient increase in intracellular ROS enhances the activity of POMC neurons and suppresses NPY/AgRP neurons, resulting in decreased food consumption and increased energy expenditure[8]. The digestive tract can be likened to a bioreactor, with ROS being produced as byproducts of the standard process of food digestion[10]. Interestingly, there is limited information on the role of ROS in food digestive processes, particularly whether neuronal ROS homeostasis impacts intestinal digestion.

In this study, we revealed an unexpected role of neuronal ROS in controlling food digestion. Through a genome-wide RNAi screen using the established food digestion system in *C. elegans*, we found that the capacity to digest food is diminished in animals where *ctl-1, ctl-2, ctl-3, sod-3*, and *prdx-2* have been knocked down. These genes influence H_2O_2 and ROS homeostasis. Interestingly, we observed that PRDX-2 knockout specifically in AWC neurons reduces the ability of animals to digest non-edible food. This happens through the activation of the peripheral UPR^{mt}, which requires the neuropeptide, NLP-1. Moreover, we showed that the ablation of AWC neurons activates intestinal UPR^{mt} and inhibits food digestion. In summary, neuronal "ROS signaling" systematically activates intestinal "eat less signaling" to shut down digestion through UPR^{mt} induction, thereby decreasing food usage to alleviate the cellular stress.

Results

ROS homeostasis as a key factor in regulating food digestion

Previously, we found that the worms arrested development at early larval stages when fed non-edible bacteria *Staphylococcus saprophyticus* (SS)[4,5]. SS was accumulated in the gut, and the intestinal lumen of worms fed SS were bloated, suggesting that worms failed to digest the SS[5]. We have established a food digestion research system where low-quality food (Heat killed-*E. coli*) activates worm to digest inedible food (SS)[5,6].

We discovered that signals such as outer membrane proteins (OMP) and peptidoglycan from heat-killed *E. coli* activate the food digestive system in worm, thereby enabling them to digest inedible food SS to support growth[5,7]. In animals, inhibition of the conserved innate immune signaling, PMK-1, stimulates food digestion, demonstrating a prominent role of the innate immune pathway in digestion system[5].

To discover other signals involved in digestion regulation, we could perform an RNAi screen and identified the genes that positively regulation food digestion. After knocking down these genes, HK-*E. coli* failed to promote worms to digest SS, resulting in animals showing a slow growth phenotype when fed HK-*E. coli* + SS food (Supplementary Fig. 1a). Through a genome-wide RNAi screen, we found that animals growth slowed by RNAi inactivation of 26 genes in HK-*E. coli* + SS feeding condition (Supplementary Fig. 1b), suggesting that these genes may be involved in promoting animals to digest SS. GO enrichment analysis shows that most enrichment genes are related to H_2O_2 and ROS homeostasis regulation (Supplementary Fig. 1c), such as *ctl-1*, *ctl-2*, *ctl-3*, *sod-3* and *prdx-2*, suggesting that ROS homeostasis may be a key factor in animals for regulating food digestion.

To confirm this hypothesis, (i) we quantified the oxidative status in animals utilizing the redox-sensitive dye MitoTracker™ Red CMXRos (further details provided in the methods section). This dye is highly sensitive to alterations in mitochondrial membrane potential, which may be impacted by the presence of reactive oxygen species (ROS) during periods of oxidative stress[11]. We found that *ctl-1*, *ctl-2*, *ctl-3*, *sod-3* and *prdx-2* mutant animals (Supplementary Fig. 2a) are experiencing oxidative stress, indicating that reactive oxygen species (ROS) homeostasis is disrupted in these mutants; (ii) We assessed the developmental rate of mutant animals fed HK-*E. coli* + SS and found that all of these mutants grew slower than wild-type animals (Fig. 1a). However, they exhibited a slightly slower growth phenotype under normal *E. coli* OP50 feeding conditions (Supplementary Fig. 2b). Moreover, this developmental delay phenotype is suppressed by supplementation of antioxidant NAC (Fig. 1b), suggesting that food digestion ability is decreased in animals by disruption of ROS homeostasis; (iii) Moreover, we found that the supplementation of low concentration of H_2O_2 significantly suppressed development of wild-type animals by feeding with HK-*E. coli* + SS (Fig. 1c), but not under normal *E. coli* OP50 feeding conditions (Supplementary Fig. 2c), supporting the idea that oxidative stress inhibit digestion. All of the data indicate that disruption of ROS homeostasis in animals shuts down food digestion.

We next investigated whether ROS homeostasis is affected in animals feeding on non-edible or digested food. Our results showed that oxidative stress levels increased in animals fed non-edible food (SS) (Fig. 1d), suggesting that proper ROS homeostasis is crucial for the digestion process.

Peroxiredoxin 2 promotes food digestion through scavenging ROS

Peroxiredoxins (Prxs) are proteins that are highly conserved and found in most organisms. Their primary function is to scavenge reactive oxygen species (ROS)[12]. To study the role of ROS in food digestion, we began by investigating the function of Peroxiredoxins (Prdx) in food digestion. We found that mitochondrial ROS level is increased in animals with *prdx-2* mutation (Fig. 2a) or RNAi (Fig. 2b), which is consistence with PRDX-2's role in scavenging ROS within the cells. In addition to our study, other laboratories have recently demonstrated increased levels of mitochondrial ROS[13] and endogenous H_2O_2[14] in *prdx-2* mutant animals. Interestingly, we observed that *prdx-2* mutants exhibited slower growth than wild-type when fed HK-*E. coli* + SS (Fig. 2c), suggesting that food digestion ability is decreased in *prdx-2* mutant. However, the developmental delay phenotype is suppressed when the antioxidant NAC was supplemented (Fig. 2d). This implies that increased ROS in *prdx-2* mutant inhibits animals' ability to digest SS. Additionally, we observed that NAC treatment also enhanced the growth of wild-type animals (Fig. 2d), suggesting that the antioxidant NAC may promote digestion. Overall, our findings suggest that PRDX-2 enhances the ability of animals to digest SS food by scavenging ROS.

Peroxiredoxin 2 (Prdx2) plays a positive role in food digestion within the AWC neuron

To investigate the function of PRDX-2 in food digestion, we first constructed the transgenic animals to analyze the expression and localization of this gene using transgenic strains: *prdx-2p::GFP* and *prdx-2p::PRDX-2::GFP* or *prdx-2p::GFP::PRDX-2*. We observed that *prdx-2p::GFP* was expressed in head neuron, which co-localized with *odr-1p::RFP*, an AWC neuronal marker (Supplementary Fig. 3a). This suggests that *prdx-2* is expressed in the AWC neuron. In addition to the AWC neuron, *prdx-2* was also expressed in other head neuron and tail neuron, which we have not yet identified (Supplementary Fig. 3a).

Using two transgenic animals (*prdx-2p::PRDX-2::GFP* or *prdx-2p::GFP::PRDX-2*), we found that PRDX-2 also co-localized with *odr-1p::RFP* (Fig. 3a and Supplementary Fig. 3b), suggesting its localization in the AWC neuron. We also observed that PRDX-2 was expressed in the intestine and other head neuron (Fig. 3a and Supplementary Fig. 3b).

Considering that PRDX-2 is expressed in both neurons and the intestine, and that neuronal PRDX-2 plays a role in detecting H_2O_2[15] and

https://doi.org/10.1038/s41467-024-55013-3

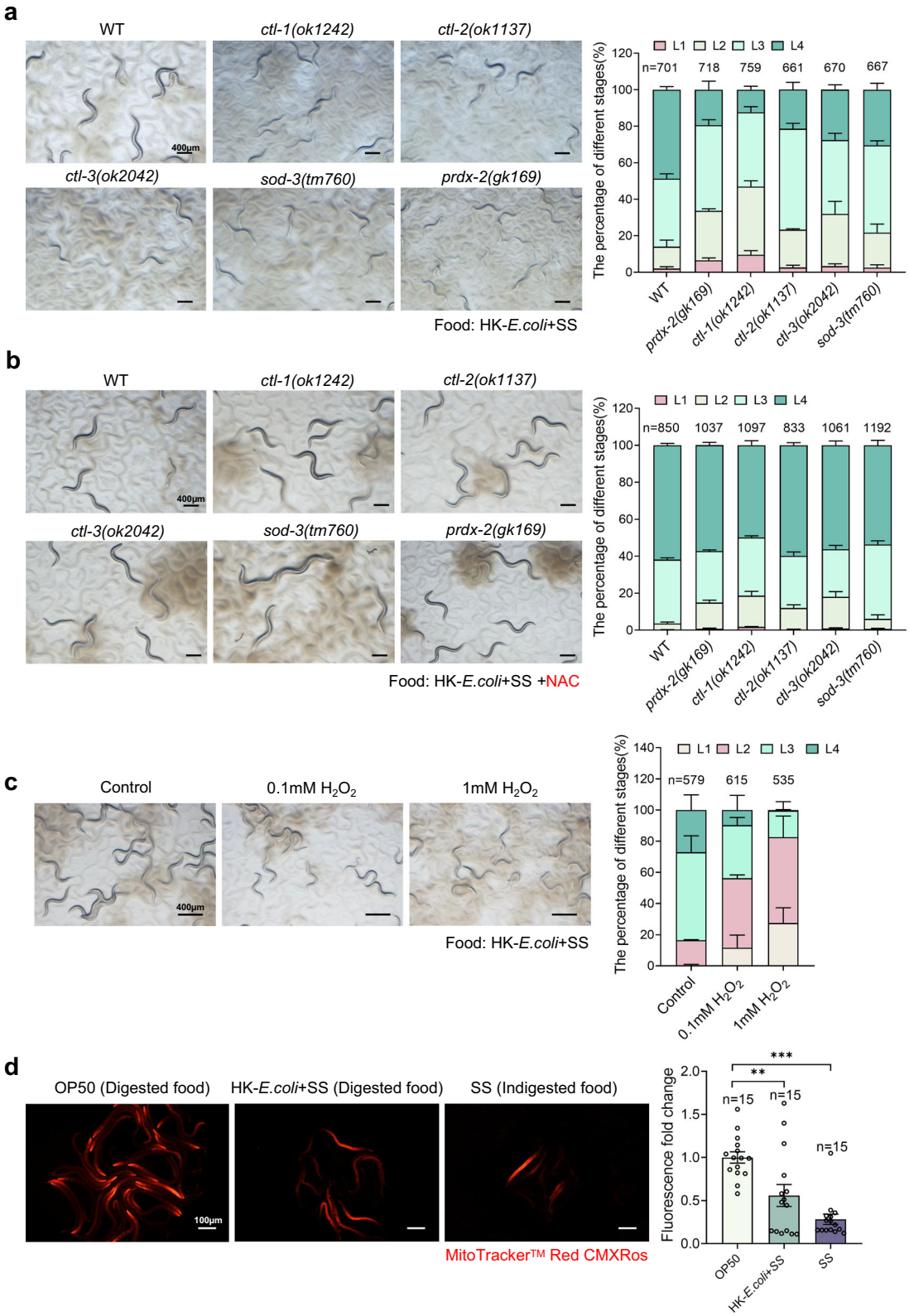

modulating H_2O_2-induced feeding[16] and behavioral responses[17], we sought to determine which tissue-specific expression of PRDX-2 is involved in regulating food digestion. We expressed *prdx-2* with pan-neuron (*rgef-1*), AWC neuron (*odr-1*), intestine (*vha-6*) and its own promoter into *prdx-2(gk169)* mutant and fed these animals with HK-*E. coli* + SS (Fig. 3b–e). We found that pan-neuron and AWC neuron expression of *prdx-2* could rescue the development defect of *prdx-2(gk169)* (Fig. 3c–e), but not in intestine (Fig. 3d). Interestingly, the high level of ROS in *prdx-2* mutant was also rescued (reduced) by expression *prdx-2* in pan-neuron and AWC neuron, but not in the intestine (Supplementary Fig. 3c). These results suggest that PRDX-2 in AWC neuron promotes food digestion by maintaining ROS homeostasis.

To further confirm the role of PRDX-2 in food digestion in AWC neuron, we specifically knocked out *prdx-2* in the AWC neuron using CRISPR-Cas9 (Supplementary Fig. 3d). We observed that (i) the oxidative stress is elevated in animals with *prdx-2* knockout specifically in

Fig. 1 | The role of ROS homeostasis in regulating food digestion. **a** Developmental progression of synchronized WT, *prdx-2(gk169)*, *ctl-1(ok1242)*, *ctl-2(ok1137)*, *ctl-3(ok2042)*, *sod-3(tm760)* L1 animals grown on HK-*E. coli* + SS bacteria for 96 h at 20°C. Obtained *p* values (from L4 stage) were as follows: WT vs *prdx-2(gk169)*; $p = 0.004$. WT vs *ctl-1(ok1242)*; $p = 0.0001$. WT vs *ctl-2(ok1137)*; $p = 0.003$. WT vs *ctl-3(ok2042)*; $p = 0.003$. WT vs *sod-3 (tm760)*; $p = 0.01$. **b** Developmental progression of different synchronized WT, *prdx-2(gk169)*, *ctl-1(ok1242)*, *ctl-2(ok1137)*, *ctl-3(ok2042)*, *sod-3(tm760)* L1 animals grown on HK-*E. coli* + SS bacteria supplemented with 50 mM NAC for 96 h at 20°C. Obtained *p* values (from L4 stage) were as follows: WT vs *prdx-2(gk169)*; $p = 0.06$. WT vs *ctl-1(ok1242)*; $p = 0.01$. WT vs *ctl-2(ok1137)*; $p = 0.29$. WT vs *ctl-3(ok2042)*; $p = 0.09$. WT vs *sod-3 (tm760)*; $p = 0.05$. **c** Developmental progression of WT synchronized L1 animals grown on HK-*E. coli* + SS bacteria supplemented with 0.1 mM, 1 mM H_2O_2 for 96 h at 20°C. Obtained *p* values (from L2 stage) were as follows: Control vs 0.1 mM H_2O_2; $p = 0.0001$. Control vs 1 mM H_2O_2; $p = 0.04$. **d** Representative microscope images and quantitative analysis of MitoTracker™ Red CMXRos fluorescent in WT animals after grown on *E. coli* OP50, HK-*E. coli* + SS, SS for 24 h. Obtained *p*-values were as follows: OP50 vs HK-*E. coli* + SS; $p = 0.005$. OP50 vs SS; $p < 0.0001$. See more detail method in the methods section. For all panels, *n* = the number of worms. Data are represented as mean ± SEM. All statistical analyses were preformed using unpaired two-tailed Student's *t*-test. $^{**}p < 0.01$, $^{***}p < 0.001$; n.s., not significant. All experiments were performed independently at least three times. Source data are provided. as a Source Data file. See also Supplementary Figs. 1, 2.

AWC neurons (Fig. 3f); (ii) animals with *prdx-2* knockout in AWC neurons exhibited slower growth compared to wild-type animals when fed HK-*E. coli* + SS (Fig. 3g). To evaluate food digestion capability, we measured the width of the intestinal lumen, a marker that becomes enlarged when digestion is impaired, as our previously reported[7]. We observed intestinal bloating in animals with a *prdx-2* mutation in whole body or in AWC neurons (Supplementary Fig. 3e), indicating a reduced ability to digest food in these mutants. This suggests that PRDX-2 in AWC promotes animals to digest SS food.

A robust activation of UPR^{mt} inhibit food digestion capacity

Mitochondria are both a major source and target of reactive oxygen species (ROS). To combat mtROS and alleviate mitochondrial stress, cellular systems have evolved a quality control mechanism known as the mitochondrial unfolded protein response (UPR^{mt})[18]. In previous studies, we found that food digestion ability decreased in *bcf-1*[7] or *afts-1 (et18)* mutant animals (Supplementary Fig. 4a), which exhibited activation of UPR^{mt}. To further validate these results, we assessed food digestion capacity in animals subjected to RNAi targeting genes known to induced by UPR^{mt} based on previous reports[19]. We observed that food digestion capacity decreased in animals undergoing RNAi of *cco-1, spg-7*, or *gfm-1*, which induce robust UPR^{mt} (Supplementary Fig. 4b, c). However, there was not a significant change in food digestion capacity in animals undergoing RNAi of *tsfm-1* or *nuaf-3*, which induce mild UPR^{mt} (Supplementary Fig. 4b, c). This data strongly suggests that robust activation of UPR^{mt} may inhibit food digestion capacity.

We also explored an alternative possibility: mitochondrial dysfunction resulting from the inhibition of the respiratory chain impairs digestion. We knocked down genes associated with the mitochondrial respiratory chain, including *atp-2, nuo-1, nuo-6, ndua-5, ndua-2, gas-1, ndub-6, sdbh-1*, and *sdhd-1*. Our findings indicated that all of these RNAi treatments induced the UPR^{mt}, with *atp-2, ndua-5, nuo-1*, and *nuo-6* RNAi leading to a strong UPR^{mt} response (Supplementary Fig. 5a). Interestingly, we observed that the food digestion capacity was not reduced in all RNAi-treated animals due to respiratory chain inhibition, suggesting that the inhibition of the respiratory chain did not directly impair digestion. However, we did find that food digestion capacity decreased in animals subjected to RNAi of *atp-2, nuo-1, nuo-6* and *ndua-5*, which induced a robust UPR^{mt} response (Supplementary Fig. 5b). These data imply that: (i) inhibition of the respiratory chain does not directly hinder digestion, and (ii) a strong activation of UPR^{mt} caused by respiratory chain inhibition suppresses food digestion capacity, whereas a mild activation of UPR^{mt} does not.

To further investigate whether this robust UPR^{mt} activation is indeed responsible for the observed digestion inhibition, we examined the digestive phenotype in *cco-1* RNAi animals carrying an *atfs-1* mutation. Our results revealed that the digestion defects present in *cco-1* RNAi animals were alleviated by the *atfs-1* mutation, which effectively abolished UPR^{mt} activation (Supplementary Fig. 5c). These findings suggest that a robust activation of UPR^{mt} plays a crucial role in inhibiting food digestion. This led us to question whether increased ROS in *prdx-2* mutant animals also induces UPR^{mt}, thereby inhibiting food digestion.

AWC-specific knockout *prdx-2* induces cell non-autonomous UPR^{mt}

UPR^{mt} induction requires the key transcription factor ATFS-1 and its transcriptional co-regulators, including DVE-1[20–22]. Our findings showed that *prdx-2* knockout induces the mitochondrial unfolded protein response (UPR^{mt}) through activation of *hsp-6* expression (Fig. 4a, Supplementary Fig. 6a) and translocation of DVE-1, a regulator of *hsp-6*[21], into the nucleus (Fig. 4b) in the intestine. This is dependent on the classical UPR^{mt} pathway, ATFS-1 (Supplementary Fig. 6b). Furthermore, UPR^{mt} was induced in animals with mutations of *ctl-2*, *ctl-3*, and *sod-3* (Supplementary Fig. 6c), which increase the ROS level in animals. To determine if *prdx-2* mutation-induced ROS specifically triggers UPR^{mt}, we also assessed the unfolded protein response in the endoplasmic reticulum (UPR^{ER}) and cytosol (UPR^{Cyt}). Our findings indicate that neither the *hsp-4p::gfp* reporter (UPR^{ER}) (Supplementary Fig. 6d) nor the *hsp-16.2p::gfp* reporter (UPR^{Cyt}) (Supplementary Fig. 6e) was induced in animals by *prdx-2* RNAi. These data suggest that *prdx-2* mutation specifically induces UPR^{mt}.

Given that PRDX-2 in neurons promotes food digestion, we wondered if neuronal PRDX-2 regulates intestinal UPR^{mt}. We found that the expression of *prdx-2* with pan-neuron (*rgef-1*) and AWC neuron (*odr-1*) strongly rescued (inhibited) the activation of *hsp-6p::GFP* in the intestine of *prdx-2* mutants (Fig. 4c). Moreover, *prdx-2* knockout in the AWC neuron also induced peripheral UPR^{mt} (Fig. 4d). These data suggest that PRDX-2 in the AWC neuron mediates cell non-autonomous UPR^{mt}.

The UPR^{mt} system consists of chaperones and proteases, which promote protein folding or eliminate mitochondrial proteins damaged by mtROS, respectively. ATFS-1 is known to be a key transcription factor involved in UPR^{mt} activation. We found that UPR^{mt} activation in *prdx-2* mutants is abolished by RNAi of *atfs-1*. Therefore, we wondered whether activated UPR^{mt} also helps or promotes animals to digest food under stress conditions, such as disruption of ROS homeostasis in *prdx-2* mutants. Under the food digestion system (HK-*E. coli* + SS feeding condition), the *prdx-2* mutant had a severe synthetic growth defect on an *afts-1* (loss-of-function) mutation background, where *atfs-1* mutant development was similar to the wild-type (Fig. 4e), suggesting that ATFS-1 is essential for survival under mitochondrial stress induced by *prdx-2* inhibition.

prdx-2 knock-out induced cell non-autonomous UPR^{mt} requires neuropeptide (NLP-1)

The mitochondrial unfolded protein response (UPR^{mt}) is triggered non-cell-autonomously through retromer-dependent Wnt signaling[23]. Specifically, when the Q40 protein is expressed in neurons of *C. elegans*, it induces UPR^{mt} activation in the intestine, a process that relies on the Wnt signaling pathway mediated by EGL-20[23]. To investigate whether UPR^{mt} induction due to *prdx-2* knockout in AWC neurons also requires EGL-20, we evaluated UPR^{mt} levels in the intestine by knocking down *egl-20* in *prdx-2* AWC knockout mutants. Surprisingly, we found

https://doi.org/10.1038/s41467-024-55013-3

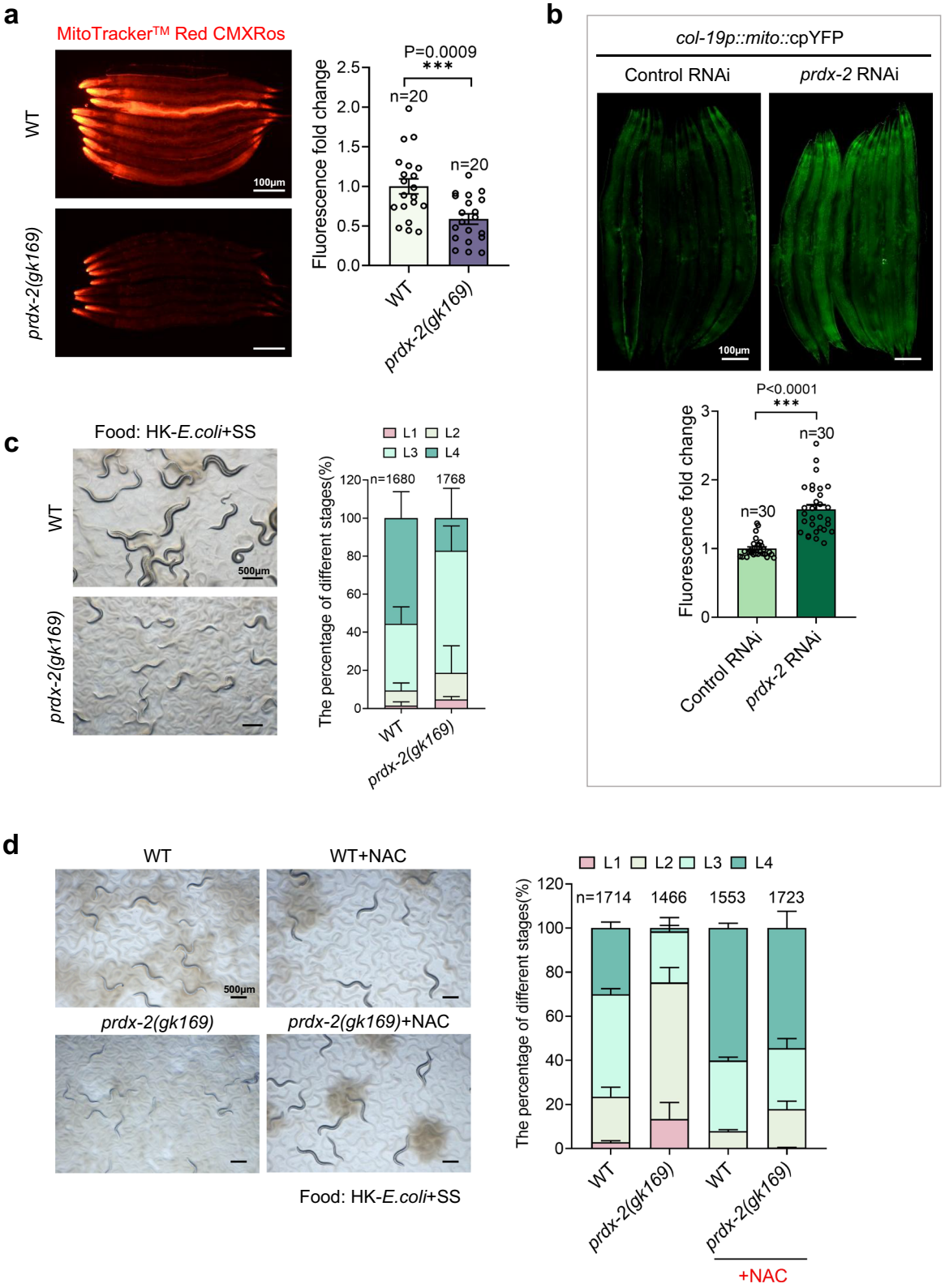

that UPR^{mt} levels did not decrease in the *prdx-2* mutant after *egl-20* RNAi treatment (Supplementary Fig. 7a). Instead, UPR^{mt} levels slightly increased in the *prdx-2* AWC knockout mutants following *egl-20* RNAi (Supplementary Fig. 7a). These results suggest that the activation of intestinal UPR^{mt} in *prdx-2* knockout in AWC neurons does not depend on the Wnt signaling pathway mediated by EGL-20.

The AWC neuron does not physically interact with the intestine, yet the AWC-specific knockout of *prdx-2* induces intestinal UPR^{mt}. This suggests that a neuroendocrine signal may be required for signaling transduction. Previous studies have shown that NLP-1, released from the AWC, is required for lowering the AWC's calcium response to odors[24]. Recent research also indicates that mtROS is necessary for NLP-1 secretion[25]. Therefore, we asked whether UPR^{mt} induction by *prdx-2* knockout also requires neuropeptide, NLP-1.

To test this, we first constructed transgenic animals (*nlp-1p::GFP*) to observe the expression pattern and found that it was expressed in

Fig. 2 | Peroxiredoxin 2 facilitates ROS clearance to promote food digestion. **a** Representative microscope images and quantitative analysis of MitoTracker™ Red CMXRos fluorescent showing increased ROS level in WT and *prdx-2(gk169)* after being grown on *E. coli* OP50 for 48 h at 20°C. Obtained *p* value was: WT vs *prdx-2(gk169)*; $p = 0.0009$. See more detail method in the methods section. **b** Representative microscope images and quantitative analysis of *col-19p::mito::cpYFP* fluorescent in WT animals treated with vector control and *prdx-2* RNAi bacteria. The *col-19p::mito::cpYFP* has been used as a sensor for Mitochondrial ROS[46]. Obtained *p* value was: Control RNAi vs *prdx-2* RNAi; $p < 0.0001$. **c** Developmental progression of synchronized WT, *prdx-2(gk169)* L1 animals grown on HK-*E. coli* + SS bacteria for 96 h at 20 °C. Obtained *p* values (from L4 stage) was: WT vs *prdx-2(gk169)*; $p = 0.03$. **d** Developmental progression of synchronized WT, *prdx-2(gk169)* L1 animals grown on HK-*E. coli* + SS bacteria supplemented with 50 mM NAC for 96 h at 20°C. Obtained *p* values (from L4 stage) were as follows: WT vs *prdx-2(gk169)*; $p < 0.0001$. WT + NAC *vs prdx-2(gk169)*+NAC; $p = 0.29$. For all panels, *n* = the number of worms. Data are represented as mean ± SEM. All statistical analyses were preformed using unpaired two-tailed Student's *t*-test.**$p < 0.01$, ***$p < 0.001$, n.s., not significant. All experiments were performed independently at least three times. Source data are provided as a Source Data file.

the AWC neuron (Fig. 5a). We then measured the mRNA level of *nlp-1* and found that *nlp-1* mRNA is increased in the *prdx-2* mutant on OP50 or HK-*E. coli* + SS feeding conditions (Fig. 5b). Based on western blot analysis using *nlp-1p::GFP* reporter strain, we observed increased *nlp-1* expression in animals subjected to *prdx-2 RNAi* (Supplementary Fig. 7b). Furthermore, we discovered that the increased UPR^{mt} in *prdx-2* mutant animals is suppressed by *nlp-1* mutation (Fig. 5c). These data suggest that *prdx-2* knockout induces intestinal UPR^{mt} through increasing the expression of NLP-1.

Next, we investigated the regulation of *nlp-1* expression. In our study, we observed that increasing ROS levels through mutations in *ctl* or *sod* genes, or by supplementing with H_2O_2, inhibits animals' food digestion. Therefore, we also explored whether ROS could influence *nlp-1* expression. We found that *nlp-1* expression was elevated in animals supplemented with H_2O_2 (Supplementary Fig. 7c), suggesting that oxidative stress induces *nlp-1* expression to inhibit digestion. Furthermore, we examined *nlp-1* expression in animals subjected to *ctl-3* and *sod-3* RNAi. We observed increased *nlp-1* expression in these animals (Supplementary Fig. 7d), indicating that ROS accumulation induces *nlp-1* expression. Overall, these findings suggest that elevated ROS levels may induce *nlp-1* expression.

To investigate the mechanism by which an increase in neuronal ROS leads to *nlp-1* expression, we examined whether this ROS-induced *nlp-1* expression relies on neurotransmission. We assessed *nlp-1* expression in animals subjected to RNAi targeting *unc-31*, a gene essential for dense core vesicle neurotransmission[26]. Our results revealed that the induction of *nlp-1* expression by *prdx-2* RNAi was inhibited by *unc-31* RNAi (Supplementary Fig. 7e), indicating that ROS-induced *nlp-1* expression is indeed dependent on neurotransmission.

To determine whether secreted NLP-1 activates UPR^{mt}, thereby regulating food digestion, we overexpressed *nlp-1* using its own promoter, the AWC neuron (*odr-1p*), and the intestinal (*vha-6*) promoter. We found that UPR^{mt} was activated in all transgenic animals (Fig. 5d), suggesting that secreted NLP-1 activates intestinal UPR^{mt}. Simultaneously, the transgenic animals with over-expressing *nlp-1* in native (Fig. 5e) or AWC neuron (Fig. 5f) grew slower than the wild-type when fed HK-*E. coli* + SS (Fig. 5e, f), suggesting that food digestion ability decreased in animals by overexpressing NLP-1. This implies that NLP-1 secretion activates the intestinal UPR^{mt}, thereby inhibiting food digestion.

Ablation of AWC neurons activate intestinal UPR^{mt} and inhibit digestion

AWC food-sensing neurons release NLP-1, which acts on the NPR-11 receptor in the AIA interneurons to modulate INS-1 insulin release. This in turn feeds back to dampen AWC olfactory responses and alter food-seeking behaviors[27]. Given that *prdx-2* functions in the AWC neuron to regulate UPR^{mt} and digestion, we hypothesized that ablation of AWC neurons could mimic a food depletion condition, potentially shutting down food digestion.

To test this, we first constructed transgenic animals that over-express *egl-1*, a cell death activator[28], in AWC neurons. This was done using the *odr-1* promoter in an *hsp-6p::GFP* background (Fig. 6a). We then crossed a previously validated transgenic strain that expresses cleaved caspase under the AWC-specific promoter, *ceh-36* (*ceh-36p::caspase*)[29], into a UPR^{mt} reporter strain (*hsp-6p::GFP*). We found that UPR^{mt} was activated in both animals with ablation of AWC (Fig. 6a, b), which consistence with recently study showing that olfactory nervous system in *C. elegans* regulates the UPR^{mt} cell nonautonomously[30]. Additionally, we observed an elevated oxidative stress in animals where AWC was ablated, as indicated by staining with the redox-sensitive dye MitoTracke™ Red CMXRos (Supplementary Fig. 8).

Next, we measured the animals' development when fed HK-*E.coli* + SS and found that animals with ablation of AWC grew slower than the wild-type (Fig. 6c, d). This suggests that the ability to digest food decreased when AWC neurons were ablated. In conclusion, these data suggest that the ablation of AWC neurons activates intestinal UPR^{mt} and inhibits food digestion.

PMK-1 contributes to the inhibitory effect of UPR^{mt} activation caused by *prdx-2* mutation on food digestion

Our previous study showed that inhibition of the innate immune PMK-1 pathway enhances digestion[5]. In our recent study, we demonstrated that PMK-1 partially mediates the inhibitory effect of UPRmt activation on food digestion[7]. Thus, we investigated whether PMK-1 also contributes to the inhibitory effect of UPR^{mt} activation caused by *prdx-2* mutation on food digestion. Firstly, we measured PMK-1 levels in *prdx-2* mutants and found that p-PMK-1 levels were elevated in *prdx-2* mutant animals under *E. coli* or HK-*E. coli* + SS feeding conditions, indicating that activation of the PMK-1 pathway may contribute to the digestive defects in *prdx-2* mutants (Supplementary Fig. 9a). Secondly, to further explore the role of the PMK-1 pathway in *prdx-2* mutant digestive defects, we generated double mutants *prdx-2(gk169);pmk-1(km25)* and observed that the developmental delay (food digestion defects) in *prdx-2* mutants was rescued in the double mutants (Supplementary Fig. 9b). These results suggest that *prdx-2* mutation activates innate immunity through the PMK-1 pathway, thereby inhibiting food digestion.

Discussion

Food digestion is a multifaceted process that is crucial for maintaining health. Reactive Oxygen Species (ROS) in the hypothalamus play a role in regulating food intake and metabolism. However, it is still unclear whether neuronal ROS signaling regulates food digestion in the intestine. Here, by using an established food digestion system in *C. elegans*, we discovered that neuronal ROS (free radicals) shut down the food digestion through signaling the peripheral UPR^{mt} by neuropeptide (Fig. 6e).

Gut hormones and afferent neurons play a crucial role in regulating digestive processes such as gastric emptying and gut motility. It is widely believed that gut-brain signaling may be significant in regulating food-related physiology, including food intake, and preferences. However, our understanding of the neuronal signals that activate intestinal food digestion remains limited. Through a whole-genome RNAi screen, we identified several genes, including *ctl-1, ctl-2, ctl-3, sod-3*, and *prdx-2*, which are involved in maintaining ROS homeostasis, positively regulate food digestion. Knocking down of these genes resulted in a decrease in food digestion ability. We discovered that *prdx-2* is expressed in AWC neurons, and specifically knocking out

https://doi.org/10.1038/s41467-024-55013-3

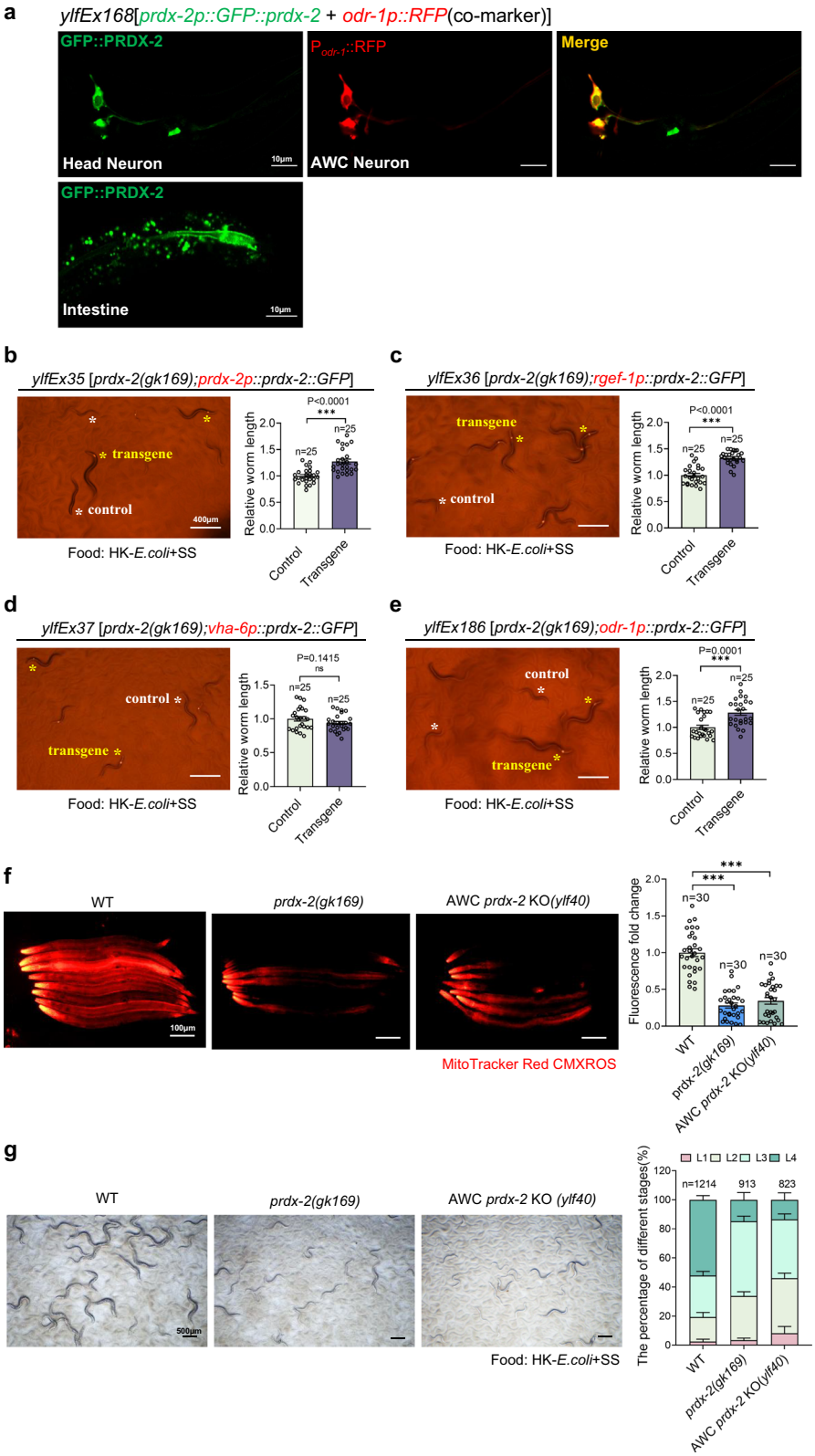

this gene in AWC neurons shuts down food digestion, suggesting that free radicals increasing in neurons shuts down digestion.

We found that food digestion ability decreases in animals when AWC neurons are ablated, indicating that AWC neurons also contribute to promoting food digestion. AWC neurons are olfactory neurons critical for chemotaxis to volatile odorants such as benzaldehyde, butanone, isoamyl alcohol[31]. These neurons also respond to temperature[32]. Recently study also show that olfactory nervous system in *C. elegans* regulates the UPR^{mt} cell nonautonomously[30].

Pathogen-associated odorants also extend lifespan through TGF-β signaling and UPR activation[33]. However, whether and how olfactory neurons respond to food and signal to the digestive system has not been reported yet. Our finding that the mutation of *prdx-2* in AWC neurons disrupts the food digestive system by inducing intestinal

Fig. 3 | *prdx-2* knock-out in AWC neuron shut down food digestion. a Confocal image of expression pattern of PRDX-2. **b**–**e** Developmental progression of *prdx-2(gk169)* carries with (**b**) *prdx-2p::prdx-2::gfp* (by its own promoter expression) or (**c**) *rgef-1p::prdx-2::gfp* (neuron-specific expression) or (**d**) *vha-6p::prdx-2::gfp* (intestine-specific expression) or (**e**) *odr-1p::prdx-2::gfp* (AWC neuron-specific expression) animals quantified by relative worm length. Animals carrying transgenes are labeled in yellow. Obtained *p* values were as follows: (**b**) Control vs Transgene; $p < 0.0001$. (**c**) Control vs Transgene; $p < 0.0001$. (**d**) Control vs Transgene; $p = 0.14$. (**e**) Control vs Transgene; $p = 0.0001$. **f** Representative microscope images and quantitative analysis of MitoTracker™ Red CMXRos in WT, *prdx-2(gk169)* or AWC neuron specific knockout *prdx-2* animals which grown on *E. coli* OP50 for 48 h at 20°C. Obtained *p* values were as follows: WT vs *prdx-2(gk169)*; $p < 0.0001$. WT vs AWC *prdx-2* KO *(ylf40)*; $p < 0.0001$. See more detail method in the methods section. **g** Developmental progression of synchronized WT, *prdx-2(gk169)* or AWC neuron specific knockout *prdx-2* animals L1 grown on HK-*E. coli* + SS bacteria for 96 h at 20°C. Obtained *p* values (from L4 stage) were as follows: WT vs *prdx-2(gk169)*; $p = 0.0004$. WT vs AWC *prdx-2 KO (ylf40)*; $p = 0.0003$. For all panels, *n* = the number of worms. Data are represented as mean ± SEM. All statistical analyses were preformed using unpaired two-tailed Student's *t*-test. $^{**}p < 0.01$, $^{***}p < 0.001$, n.s., not significant. All experiments were performed independently at least three times. Source data are provided as a Source Data file. See also Supplementary Fig. 3.

UPR^{mt} is both unexpected and promising. This discovery opens up new possibilities for understanding the complex interplay between the nervous system and digestion.

In mammals, ROS in the hypothalamus regulates food intake and metabolism by acting on different types of neurons, including proopiomelanocortin (POMC) and agouti-related protein (AgRP)/neuropeptide Y (NPY) neurons[9]. Thus, it is possible that neuronal ROS could potentially shut down the mammalian food digestion system, thereby reducing nutrient utilization. This hypothesis presents an intriguing prospect for future research studies, potentially leading to the development of treatments for digestive diseases or obesity by inhibiting the process of food digestion.

How does free radicals in AWC neurons shut down food digestion? Previously, we found that activation of intestinal UPR^{mt} inhibits food digestion[7]. Here, we discovered that specifically knocking out *prdx-2* in olfactory neurons (AWC) activates the intestinal unfolded protein response (UPR^{mt}), a process that requires the neuropeptide, NLP-1. Over-expressing *nlp-1* or ablating AWC neurons also activates UPR^{mt}, suggesting that free radicals in AWC neurons inhibit food digestion by activating this mitochondrial stress signal. Previous studies have demonstrated that the loss of *prdx-2* enhances stress resistance[34] and decreases insulin secretion, leading to elevated activities of DAF-16 and SKN-1[35]. More recently, research has uncovered a new role for mitochondrial-derived H_2O_2 in regulating the secretion of the neuropeptide FLP-1[36], which serves as a neuroendocrine signal during stress, activating oxidative stress responses in distant tissues. Additionally, secretion of FLP-2 is increased in *prdx-2* mutant animals, which results in elevated levels of endogenous hydrogen peroxide[14]. Therefore, it is plausible that mutations in *prdx-2* could also affect food digestion through alternative pathways, such as reducing insulin secretion or increasing FLP-2 secretion. Investigating these possibilities will be crucial for future studies in this field.

The mitochondrial unfolded protein response (UPR^{mt}) is activated when mitochondrial integrity and function are compromised. This response promotes cell survival and the recovery of the mitochondrial network to ensure optimal cellular function[18]. The cell-non-autonomous mitochondrial stress signal between neurons and the intestine in *C. elegans* has been well studied. Intestinal UPR^{mt} can be induced in animals by disrupting neuronal function, such as by neuronal knockdown of the mitochondrial electron transport chain (ETC) subunit cytochrome c oxidase-1 (cco-1)[37], neuronal expression of the Huntington's disease-causing polyglutamine protein (Q40)[38], neuronal depletion of the *C. elegans* mitofusin (FZO-1)[39], or expression of reactive oxygen species (ROS)-generating fluorescent protein KillerRed in neurons[40]. Shao et al.'s study[40] showed that antioxidant NAC or ascorbic acid treatment suppressed KillerRed-induced non-autonomous UPR^{mt}. Thus, mitochondrial ROS generated in the nervous system could potentially initiate the intestinal cell protection process, UPR^{mt}. Consistent with previous studies, we discovered that the knockout of the ROS regulation gene, PRDX-2, in olfactory neurons (AWC), triggers the activation of intestinal UPR^{mt}, thereby inhibiting food digestion. This system may serve as a protective mechanism for organisms, as "eating less" is generally beneficial for animals under stress condition.

Mitochondria, being the primary organelles responsible for energy production, play a crucial role in cellular function. The neural control of visceral organ function is vital for maintaining homeostasis and health. Consequently, we propose that neuronal ROS, indicative of neuronal mitochondrial damage, could be a highly conserved signal across species. This neuronal "damage signal-ROS" systematically activates intestinal UPR^{mt} for initiating the "eat less" response by inhibiting food digestion, thereby protecting the organism under stress condition. By shutting down food digestion, animals potentially mimic the effects of dietary restriction, thereby reducing nutrient utilization. This could lead to a reduction in protein translation, which in turn alleviates the intestinal UPR response.

In our study, we observed elevated mitochondrial ROS (mitROS) in *prdx-2* mutant animals, which correlates with impaired food digestion. Previous research has shown that PRDX-2 is essential for normal longevity[34]. Building on these findings, we asked whether *prdx-2* mutants might display heightened vulnerability to illness, resulting in food digestion inhibition. To explore this hypothesis, we present two sets of data: (i) In our recent study, we demonstrated that PMK-1 partly mediates the inhibitory effect of UPR^{mt} activation on food digestion[7]. We observed increased levels of phosphorylated PMK-1 (p-PMK-1) in *prdx-2* mutant animals. Moreover, by generating *prdx-2(gk169);pmk-1(km25)* double mutants, we observed a rescue of the developmental delay (food digestion defects) observed in prdx-2 mutants alone (Supplementary Fig. 9b). These results indicate that the *prdx-2* mutation activates innate immunity through the PMK-1 pathway, thereby inhibiting food digestion. (ii) We also evaluated the lifespan of mutant animals. Consistent with published data[34], *prdx-2* mutants exhibited a shortened lifespan, similar to *pmk-1* mutants. Intriguingly, *prdx-2(gk169);pmk-1(km25)* double mutant animals showed an even further reduction in lifespan compared to either single mutant (Supplementary Fig. 9c). Based on the lifespan data (Supplementary Fig. 9c), double mutants could be considered more susceptible ("sicker") animals due to their shortened lifespan phenotype. If *prdx-2* mutants were indeed "sicker" and inhibited in food digestion, we would anticipate that *prdx-2(gk169);pmk-1(km25)* double mutants would exhibit a food digestion defect similar to *prdx-2* mutants. However, we found that *prdx-2(gk169);pmk-1(km25)* double mutants were capable of digesting inedible food (SS), unlike *prdx-2* mutants. Therefore, our data suggest that the initial hypothesis—that *prdx-2* mutants are "sicker" animals leading to food digestion inhibition—may not be supported.

In summary, our study unveils a mechanism of brain-gut communication in regulating food digestion. In this system, neuronal "ROS signaling" systematically activates intestinal "eat less signaling", shutting down digestion through UPR^{mt} induction, thereby decreasing food usage. Our findings also suggest that regulating ROS signaling in

https://doi.org/10.1038/s41467-024-55013-3

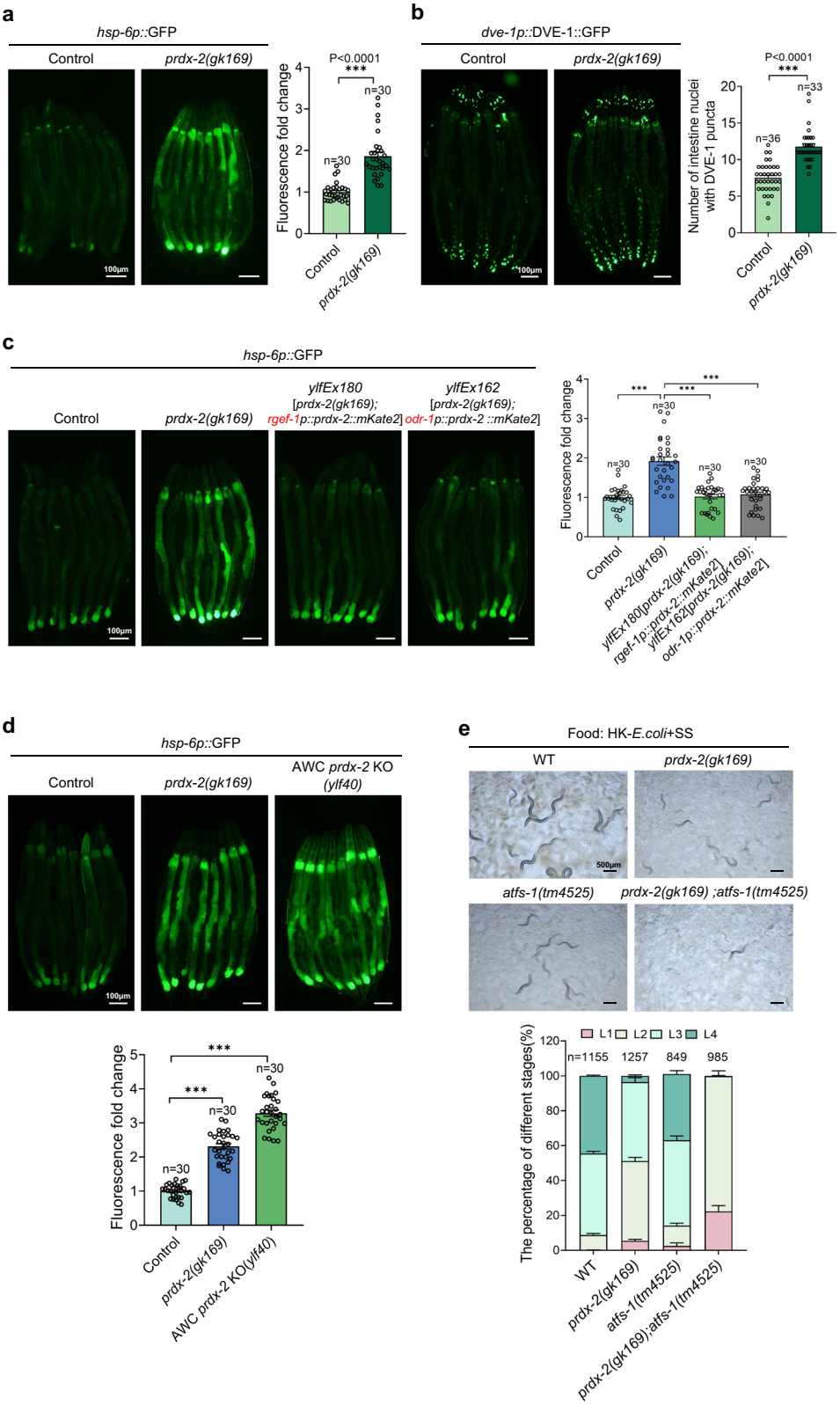

neurons could potentially serve as a therapeutic strategy for treating digestive diseases or obesity by inhibiting food digestion.

Methods

C. elegans strains and maintenance

Nematode stocks were maintained on nematode growth medium (NGM) plates seeded with bacteria (*E. coli* OP50) at 20 °C. See all the strains in Supplementary Table 1.

Bacterial strains

coli-OP50 and *Staphylococcus saprophyticus* were cultured at 37 °C in LB medium. A standard overnight cultured bacteria was then spread onto each Nematode growth media (NGM) plate.

Generation of transgenic strains

To construct the *C. elegans* plasmid for expression of *prdx-2*, 1083 bp promoter and genomic DNA of *prdx-2* was inserted into the pPD49.26-

Fig. 4 | AWC-specific knockout *prdx-2* activates intestinal UPR^{mt}. **a** Representative microscope images and quantitative analysis of *hsp-6p*::GFP expression in WT and *prdx-2(gk169)* animals. Obtained *p* value was: WT vs *prdx-2(gk169)*; $p < 0.0001$. **b** Representative microscope images and quantitative analysis of *dve-1p*::DVE-1::GFP in WT and *prdx-2(gk169)* animals. Obtained *p* value was: WT vs *prdx-2(gk169)*; $p < 0.0001$. **c** Representative microscope images and quantitative analysis of *hsp-6p*::GFP expression in WT, *prdx-2(gk169)*, *prdx-2(gk169)* carries with *rgef-1p::prdx-2::mKate2* or *odr-1p::prdx-2:: mKate2* animals. Obtained *p* values were as follows: WT vs *prdx-2(gk169)*; $p < 0.0001$. *prdx-2(gk169)* vs *ylfEx180 [prdx-2(gk169); rgef-1p::prdx-2::mKate2]*; $p < 0.0001$. *prdx-2(gk169)* vs *ylfEx162 [prdx-2(gk169); odr-1p::prdx-2::mKate2]*; $p < 0.0001$. **d** Representative microscope images and quantitative analysis of *hsp-6p*::GFP expression in WT, *prdx-2(gk169)* or AWC neuron specific knockout *prdx-2* animals. Obtained *p* values were as follows: WT vs *prdx-2(gk169)*; $p < 0.0001$. WT vs AWC *prdx-2* KO *(ylf40)*; $p < 0.0001$. **e** Developmental progression of synchronized WT, *prdx-2(gk169)*, *atfs-1(tm4525)*, *prdx-2(gk169);atfs-1(tm4525)* L1 animals grown on HK-*E. coli* + SS bacteria for 96 h at 20°C. Obtained *p* values (from L4 stage) were as follows: WT vs *prdx-2(gk169)*; $p < 0.0001$. WT vs *atfs-1(tm4525)*; $p = 0.03$. *prdx-2(gk169)* vs *prdx-2(gk169);atfs-1(tm4525)*; $p = 0.004$. For all panels, *n* = the number of worms. Data are represented as mean ± SEM. All statistical analyses were preformed using unpaired two-tailed Student's *t*-test. ***$p < 0.001$, n.s., not significant. All experiments were performed independently at least three times. Source data are provided as a Source Data file. See also Supplementary Figs. 4–6.

GFP vector. DNA plasmid mixture containing *prdx-2p::prdx-2::GFP* (10 ng/μl) and *odr-1p::RFP*(50 ng/μl) was injected into the gonads of adult N2.

To construct the *C. elegans* plasmid for expression of *prdx-2*, 1083 bp promoter and 1296 bp genomic DNA of *prdx-2* was inserted into the pPD49.26-GFP vector. DNA plasmid mixture containing *prdx-2p::prdx-2::GFP* (10 ng/μl) and *odr-1p::RFP*(50 ng/μl) was injected into the gonads of adult *prdx-2(gk169)*.

To construct the *C. elegans* plasmid for expression of *prdx-2* in neuron, 3057 bp promoter of *rgef-1* and 1296 bp genomic DNA of *prdx-2* was inserted into the pPD49.26-GFP vector. DNA plasmid mixture containing *rgef-1p::prdx-2::GFP* (10 ng/μl) and *odr-1p::RFP* (50 ng/μl) was injected into the gonads of adult *prdx-2(gk169)*.

To construct the *C. elegans* plasmid for expression of *prdx-2* in intestine, 1593 bp promoter of *vha-6* and 1296 bp genomic DNA of *prdx-2* was inserted into the pPD49.26-GFP vector. DNA plasmid mixture containing *vha-6p::prdx-2::GFP* (10 ng/μl) and *odr-1p::RFP* (50 ng/μl) was injected into the gonads of adult *prdx-2(gk169)*.

To evaluate the expression level of *hsp-6p*::GFP in *prdx-2(gk169)* after *rgef-1p::prdx-2::mKate2* supplementation, 3057 bp promoter of *rgef-1* and 1296 bp genomic DNA of *prdx-2* was inserted into the pPD49.26-mKate2 vector. DNA plasmid mixture containing *rgef-1p::prdx-2::mKate2* (10 ng/μl) and pRF4*(rol-6)* (50 ng/μl) was injected into the gonads of adult *prdx-2(gk169); zcIs13[hsp-6p::GFP + lin-15(+)]*.

To construct the *C. elegans* plasmid for expression of *prdx-2* in AWC neuron, 1348 bp promoter of *odr-1* and 1296 bp genomic DNA of *prdx-2* was inserted into the pPD49.26-GFP vector. DNA plasmid mixture containing *odr-1p::prdx-2::GFP*(10 ng/μl) and *odr-1p::RFP*(50 ng/μl) was injected into the gonads of adult *prdx-2(gk169)*.

To evaluate the expression level of *hsp-6p*::GFP in *prdx-2(gk169)* after *odr-1p::prdx-2:: mKate2* supplementation, 1348 bp promoter of *odr-1* and 1296 bp genomic DNA of *prdx-2* was inserted into the pPD49.26-mKate2 vector. DNA plasmid mixture containing *odr-1p::prdx-2::mKate2*(10 ng/μl) and pRF4*(rol-6)* (50 ng/μl) was injected into the gonads of adult *prdx-2(gk169);zcIs13*[*hsp-6p::GFP + lin-15(+)*].

To construct the *C. elegans* plasmid for expression of *prdx-2* in GFP C-terminal, 1083 bp promoter and 1296 bp genomic DNA of *prdx-2* was inserted into the pPD49.26-GFP vector. DNA plasmid mixture containing *prdx-2p::GFP::prdx-2* (10 ng/μl) and *odr-1p::RFP* (50 ng/μl) was injected into the gonads of adult *prdx-2(gk169)*.

To construct the *C. elegans* plasmid for tracking original expression of *prdx-2*, 1083 bp promoter was inserted into the pPD49.26-GFP vector. DNA plasmid mixture containing *prdx-2p::GFP*(10 ng/μl) and *odr-1p::RFP*(50 ng/μl) was injected into the gonads of adult N2.

To construct the *C. elegans* plasmid for killing AWC neuron and evaluating expression level of *hsp-6p*::GFP, 1348 bp promoter of *odr-1* and 875 bp genomic DNA of *egl-1* was inserted into the pPD49.26-mKate2 vector, DNA plasmid mixture containing *odr-1p::egl-1::mKate2* (10 ng/μl) and pRF4*(rol-6)* (50 ng/μl) was injected into the gonads of adult N2.

To construct the *C. elegans* plasmid for tracking original expression of *nlp-1*, 2019bp promoter was inserted into the pPD49.26-GFP vector. DNA plasmid mixture containing *nlp-1p::GFP*(10 ng/μl) and *odr-1p::RFP*(50 ng/μl) was injected into the gonads of adult N2.

To evaluate the expression level of *hsp-6p*::GFP after *nlp-1p::nlp-1::3*Flag* supplementation, 2019bp promoter and 691 bp genomic DNA of *nlp-1* was inserted into the pPD49.26-3*Flag vector. DNA plasmid mixture containing *nlp-1p::nlp-1::3*Flag* (10 ng/μl) and *odr-1p::RFP*(50 ng/μl) was injected into the gonads of adult *zcIs13*[*hsp-6p::GFP + lin-15(+)*].

To evaluate the expression level of *hsp-6p*::GFP after *odr-1p::nlp-1::3*Flag* supplementation, 1348 bp promoter of *odr-1* and 691 bp genomic DNA of *nlp-1* was inserted into the pPD49.26-3*Flag vector. DNA plasmid mixture containing *odr-1-1p::nlp-1::3*Flag* (10 ng/μl) and *odr-1p::RFP*(50 ng/μl) was injected into the gonads of adult *zcIs13*[*hsp-6p::GFP + lin-15(+)*].

To evaluate the expression level of *hsp-6p*::GFP after *vha-6p::nlp-1::3*Flag* supplementation, 1593 bp promoter of *vha-6* and 691 bp genomic DNA of *nlp-1* was inserted into the pPD49.26-3*Flag vector. DNA plasmid mixture containing *vha-6p::nlp-1::3*Flag* (10 ng/μl) and *odr-1p::RFP*(50 ng/μl) was injected into the gonads of adult *zcIs13*[*hsp-6p::GFP + lin-15(+)*].

See all the primers in Supplementary Table 2.

Generation *prdx-2* tissue specific knock out strain and Genotyping

To construct the *C. elegans* plasmid for knock out of *prdx-2* in AWC neuron, 600 bp promoter of *eft-3* was replaced by 1348 bp promoter of *odr-1* and *prdx-2* sgRNA was also inserted into the same CRISPR-Cas9-sgRNA vector pDD162[41]. The Cas9 target sites were designed via CRISPR design tool (http://crispor.tefor.net/) and the sgRNA sequences was 5′-CGCCTTCTCTGACCGTGCTGAGG-3′. Knockout strains were generated by injecting 25 ng/μl Cas9-sgRNA plasmid, 2 μM repair template, co-injection markers include 20 ng/μl *dpy-10* Cas9-sgRNA plasmid and 2 μM *dpy-10* repair template.

Worms were picked into 10 μl of worm lysis buffer (50 mM KCl,10 mM Tris-HCl pH 8.0, 2.5 mM $MgCl_2$, 0.45% NP40, 0.45% Tween-20, 0.01% Gelactin, 0.2 mg/mL Proteinase K), quickly freeze-thaw three times using liquid nitrogen, incubated it at 60 °C for 90 min and 95 °C for 20 min. 1 μl supernatant was taken and performed for PCR analysis with the following primers:

prdx-2: forward 5′-catttcgtcctccgatttttttct-3′,reverse 5′-gggcggtctaggaaagtgaca-3′, then digested with NheI endonuclease overnight and identified by DNA agarose electrophoresis.'

Preparation of heat-killed E. *coli* (HK-E. *coli*) + *S. saprophyticus* Food

HK-E. *coli* was prepared by our established protocol[4,42]: E. *coli* OP50 grown in LB with a standard overnight culture condition. Concentrate the cultured bacteria tenfold and then heat-killed at 80 °C for 120 min.

S. saprophyticus was prepared by our established protocol[6]: *S. saprophyticus* (SS) grown in LB with a standard overnight culture condition. Inoculate the cultured bacteria into fresh LB (1:100 ratio), 37 °C grew to $OD_{600} = 0.5$.

https://doi.org/10.1038/s41467-024-55013-3

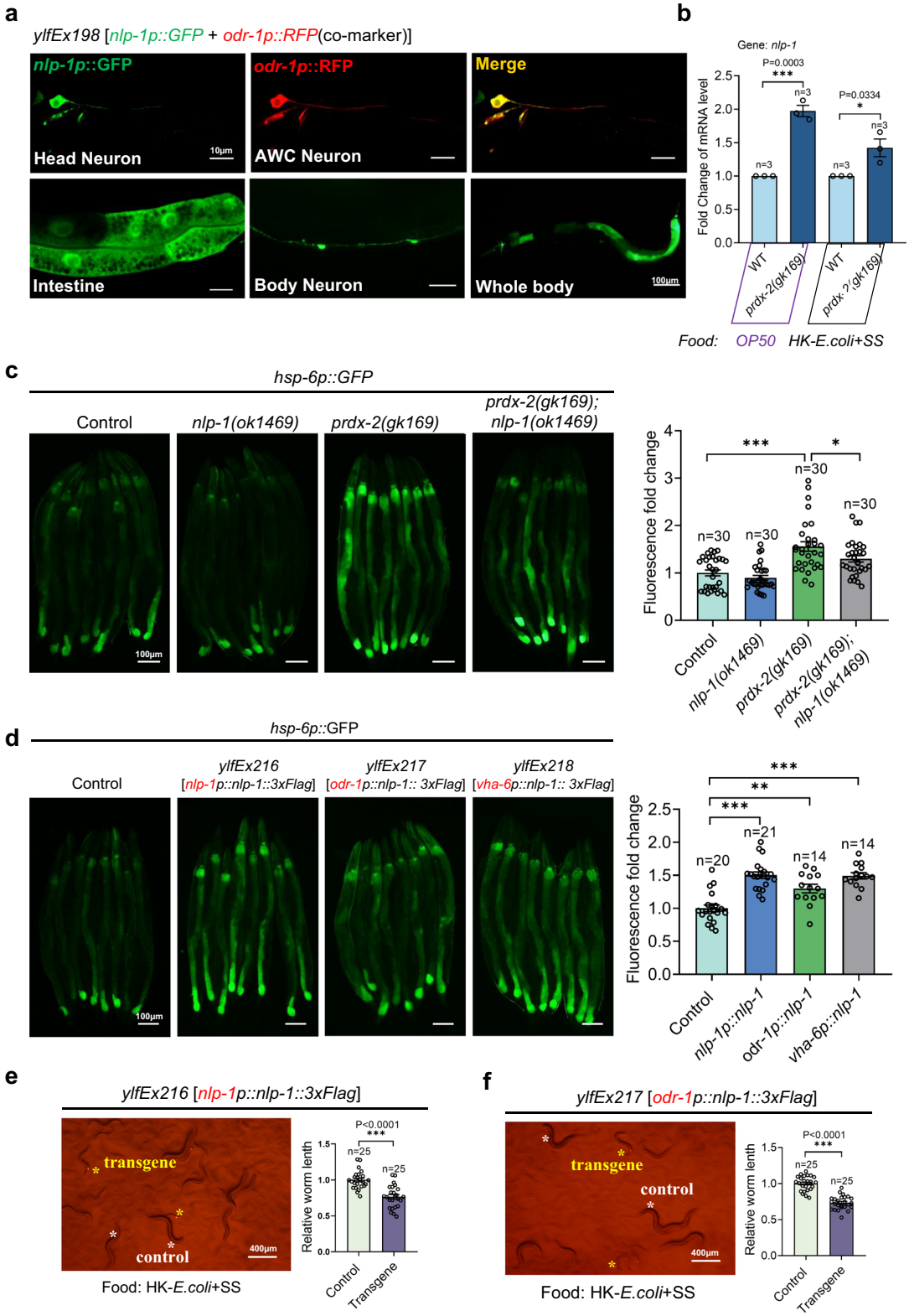

HK-E. *coli* + *S. saprophyticus* was prepared by our established protocol[5]: HK-E. *coli* and *S. saprophyticus* (SS) were mixed at a 1:1 ratio, then spread the mixture on the NGM plates.

Analysis of larval growth

C. elegans were grown on E. *coli* OP50 until to egg-laying adult and then washing in M9 buffer. Eggs were collected by bleaching, then hatched in M9 buffer for 12–16 h. Synchronized L1 larvae were seeded to plates prepared for the specific assay and incubated at 20 °C for 3–4 days.

We employed vulval morphology to determine the stage of L4 and adult animals. However, we used the length of the animals' gonads to determine stages L1–L3, following the methodology outlined in our published paper[4].

In this study, we focused exclusively on worm length for analyzing the growth of transgenic animals (as shown in Figs. 3b–e, 5e, f, 6c).

Fig. 5 | Neuropeptide NLP-1 is required for *prdx-2*-knockout-induced UPR^{mt}. **a** Confocal image of expression pattern of *nlp-1*. **b** qRT-PCR analyses of *nlp-1* mRNA level in the WT or *prdx-2(gk169)* animals feeding OP50 or HK-*E. coli* + SS. Obtained p values were as follows: WT OP50 vs *prdx-2(gk169)* OP50; $p = 0.0003$. WT HK-*E. coli* + SS vs *prdx-2(gk169)* HK-*E. coli* + SS; $p = 0.0334$. **c** Representative microscope images and quantitative analysis of *hsp-6p*::GFP expression in WT, *prdx-2(gk169)*, *nlp-1(ok1469)*, *prdx-2(gk169);nlp-1(ok1469)* animals. Obtained p values were as follows: WT vs *prdx-2(gk169)*; $p < 0.0001$. *prdx-2(gk169)* vs *prdx-2(gk169);nlp-1(ok1469)*; $p = 0.0372$. **d** Representative microscope images and quantitative analysis of *hsp-6p*::GFP expression in WT, WT carries with *nlp-1p:: nlp-1::3xFlag*, *odr-1p:: nlp-1::3xFlag* and *vha-6p::nlp-1::3xFlag* animals. Obtained *p* values were as follows: WT vs *ylfEx216[nlp-1p::nlp-1::3xFlag]*; $p < 0.0001$. *ylfEx217[odr-1p::nlp-1:: 3xFlag]*; $p = 0.001$. *ylfEx218[vha-6p::nlp-1:: 3xFlag]*; $p < 0.0001$. **e**, **f** Developmental progression of synchronized WT animals carries with *nlp-1p:: nlp-1::3xflag* (**e**) or *odr-1p:: nlp-1::3xflag* (**f**) L1 animals, which was quantified as relative worm length. Transgene worms are indicated by a yellow asterisk. Obtained *p* values were as follows: (**e**): Control vs Transgene; $p < 0.0001$. (**f**): Control vs Transgene; $p < 0.0001$. For the panels (**c**–**f**) *n* = the number of worms. For panels (**b**), *n* = the number of qPCR experiments performed. Data are represented as mean ± SEM. All statistical analyses were preformed using unpaired two-tailed Student's *t*-test. $^{*}p < 0.05$, $^{**}p < 0.01$, $^{***}p < 0.001$, n.s., not significant. All experiments were performed independently at least three times. Source data are provided as a Source Data file. See also Supplementary Fig. 7.

When constructing transgenic animals using extrachromosomal arrays, our populations often included both transgenic and non-transgenic individuals. Due to limitations in obtaining a large number of transgenic animals for certain strains, we conducted measurements of individual worm lengths for both transgenic and control (non-transgenic) animals.

C. elegans RNAi screen

All RNAi by feeding used bacterial clones from the MRC RNAi library[43] or the ORF-RNAi Library[44]. RNAi plates were prepared by adding IPTG to a final concentration of 0.024 mg/mL and Ampicillin to a final concentration of 0.1 mg/mL to NGM agar. Overnight cultured RNAi strains (LB containing 0.1 mg/mL Ampicillin and tetracycline) and the control strain (HT115 strain with empty L4440 vector) were seeded into RNAi feeding plates and cultured at room temperature for 1 days before use.

Synchronized L1 wildtype N2 worms were seed into the RNAi feeding plates for the first generation and grew until to egg-laying adult. Bleached the adult worms and collect the eggs and hatched in M9 buffer for 12–16 h. Synchronized L1 larvae were seeded on the indicated feeding plate (HK-E. *coli* + SS). The worm development stage was measured after culturing 3–4 days at 20 °C. After knocking down the genes involving in food digestion regulation, HK-*E. coli* failed to promote worms to digest SS, resulting in animals showing a slow growth phenotype when fed HK-*E. coli* + SS food (Supplementary Fig. 1a).

Worm total protein extraction

Worms were washed into the tube and the M9 Buffer were washed 3 times to remove the bacteria. Add protein lysis buffer (50Mm Tris-HCL pH 8.0, 50Mm NaCl, 0.5% deoxycholate, 10% glycerol, 1% NP40) containing PMSF (1 mM), cocktail (MCE, HY-K0011), phosphate stop (MCE, HY-K0021). Grind and break worms, centrifuge at 14000 g, 4 °C for 10 min, collected the supernatant. Used the Pierce BCA protein assay kit (Thermo Fisher, 23227) to measure the protein concentration and quantification.

Western blot

Add 5 × SDS loading buffer to the quantified protein sample (1:4), 100 °C, 10 min for denatures proteins. Then run SDS-polyacrylamide gel electrophoresis (SDS-PAGE) to separate the proteins and transfer it to the PVDF membrane. To measure the level of GFP, probed with anti-GFP (dilution = 1:3000; Proteintech, 50430-2-AP) or anti-tubulin (dilution = 1:5000; Sigma T5168) as a loading control. To measure the level of p-PMK-1, probed with anti-p-p38(dilution = 1:3000; Cell Signaling, 4511S) and anti-p38(dilution = 1:3000; Cell Signaling, 9212S) or anti-tubulin (dilution = 1:5000; Sigma T5168) as a loading control.

Oxidative stress detection of C. elegans

MitoTracker™ Red CMXRos is commonly used in oxidative stress studies to assess mitochondrial health[11]. This dye is sensitive to changes in mitochondrial membrane potential, which can be affected by the presence of reactive oxygen species (ROS) during oxidative stress. A drop in fluorescence intensity indicates a loss of mitochondrial membrane potential, reflecting mitochondrial dysfunction, which is often observed in cells experiencing elevated levels of ROS[11]. In contrast, healthy mitochondria maintain strong fluorescence under stress conditions, indicating their functionality remains intact. When mitochondrial ROS production is excessive, leading to oxidative damage, the mitochondrial membrane potential diminishes, resulting in reduced dye staining and decreased fluorescence[45].

1 mM stock solution of MitoTracker™ Red CMXRos was prepared in DMSO. Next, 0.4 μL of the stock solution was added to 50 μL of M9 buffer and thoroughly mixed. Approximately 20–30 worms were then introduced into the mixture and incubated in the dark for 5–10 min. Following this incubation period, the worms were placed on OP50 agar plates at 20 °C to recover for 30 min. Finally, the fluorescence intensity was assessed and recorded.

N-Acetyl-L-cysteine (NAC) supplementation

500 mM stock solution of N-Acetyl-L-cysteine (SIGMA, A7250-5G) was made in ddH_2O. NAC stock solution was added into NGM plates' medium with a final concentration of 50 mM before pouring of the plates. Spread the HK-E. *coli* + SS on the plates. Synchronized L1 larvae were seeded to plates and observe its development rates.

Hydrogen peroxide treatment

A 10 mM stock solution of H_2O_2 was diluted in ddH_2O. Dilute the H_2O_2 stock solution to 0.1 mM and 1Mm in M9 buffer. Synchronized L1 larvae were added into the M9 Buffer (as control)、0.1 mM H_2O_2、1 mM H_2O_2 and incubated in a shaking incubator at 20 °C for 30 min. After incubation, wash animals 3 times with M9 Buffer. Then worms were seeded to plates and observe its development rates.

Real-time PCR

Sample preparation: Synchronized L1 worms feed different foods (*E. coli* OP50 or HK-E. *coli* + SS) to L4, then worms were collected and wash 3 times with M9 Buffer to remove bacteria.

RNA isolation: The prepared samples (50 μl) were added 500 μl TRIzol (Invitrogen) and preserved at -80 °C until RNA isolation. First, blow the sample 50–100 times with a 1 ml fine needle to break the worms. Then add 100 μl chloroform and shake for 15 s, stood 5 min at room temperature, centrifuged at 14000 g, 4 °C for 15 min. Absorbent supernatant and add isopropanol (1:1), stood 10 min at room temperature, centrifuged at 14000 g, 4 °C for 10 min. Leave the precipitate and wash it with 75% ethanol. Total RNA was obtained by blow-drying precipitation and dissolved with RNA-free water.

cDNA synthesis: 1 μg RNA was reverse transcription with oligo dT primer using the PrimeScript™ II 1st Strand cDNA Synthesis Kit (Takara, 6210 A).

qPCR reaction: Gene expression levels was detected by using PowerUp™SYBR™ Green (ThermoFisher A25742) on real-time PCR

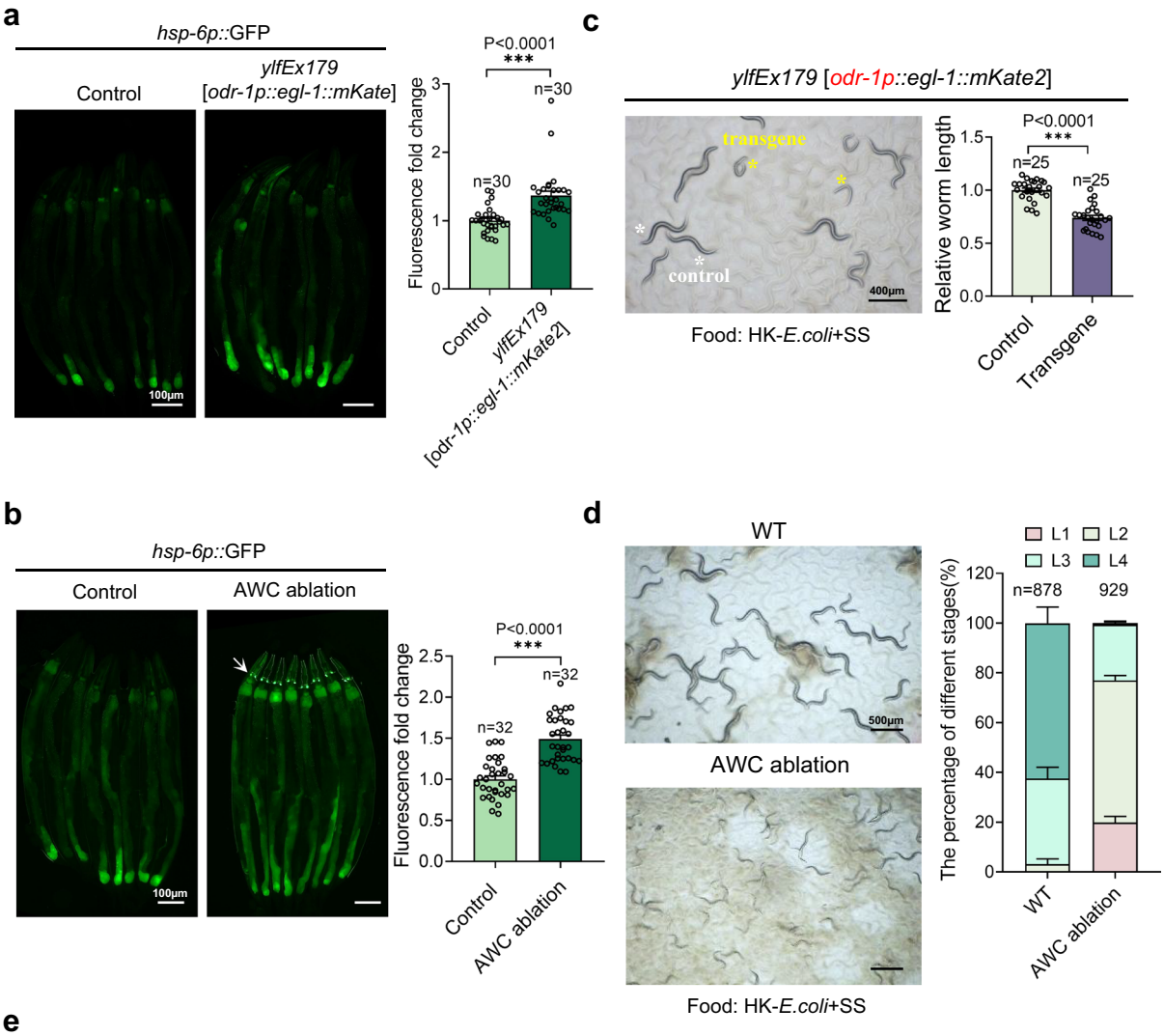

machine (ABI QuantStudio I). Fold changes in gene expression were calculated using the 2-ΔΔCt method. Primer sequences:

nlp-1: fwd 5′-TGTCTTCTTGTGATAGCTGCTG-3′ and rev 5′-GGTC GAGTACGTGAATGATGA -3′,

act-1: fwd 5′-GTTGCCGCTCTTGTTGTAGAC-3′ and rev 5′-GGTGA CGATACCGTGCTCAA-3′.

Fluorescence intensity measurement

To measure fluorescence in UPR^{mt} (*hsp-6p::GFP*), UPR^{ER} (*hsp-4p::GFP*), and UPR^{Cyt} (*hsp-16.2p::GFP*) phenotypes, worms were anesthetized with 10 mM levamisole and imaged under excitation light. Fluorescence intensity across the whole worm was quantified using ImageJ, focusing specifically on intestinal fluorescence.

Fig. 6 | Ablation of AWC neurons induce UPR^{mt} and inhibit food digestion. **a** Representative microscope images and quantitative analysis of *hsp-6p*::GFP expression in WT and WT carries with *odr-1p:: egl-1::mKate2* animals. Obtained *p* value was: WT vs *ylfEx179[odr-1p::egl-1::mKate2]*; $p < 0.0001$. **b** Representative microscope images and quantitative analysis *hsp-6p*::GFP expression in WT, animals with AWC ablation. Animals with AWC ablation (PY7502 strain) contains *srtx-1p::GFP*, which serves as a co-injection marker expressed in AFD neurons (arrow). Obtained *p* value was: WT vs AWC ablation; $p < 0.0001$. **c** Developmental progression of synchronized L1 animals (WT and WT carries with *odr-1p::egl-1::mKate2*) grown on HK-*E. coli* + SS bacteria for 96 h at 20 °C. Obtained *p* value was: Control vs Transgene; $p < 0.0001$. **d** Developmental progression of synchronized L1 animals [WT and AWC (-)] grown on HK-*E. coli* + SS bacteria for 96 h at 20 °C. Obtained *p* value (from L4 stage) was: WT vs AWC ablation; $p < 0.0001$. **e** A model for the function of neuronal ROS in regulation of food digestion in intestine. Specific knockout of PRDX-2 in olfactory neurons (AWC) leads to increased ROS levels. This triggers the release of the neuropeptide (NLP-1) and induces the intestinal UPR^{mt}, which in turn shuts down food digestion. (Created by the Qian Li using Adobe Illustrator 2020). For all panels, *n* = the number of worms. Data are represented as mean ± SEM. All statistical analyses were preformed using unpaired two-tailed Student's *t*-test. ***$p < 0.001$ n.s., not significant. All experiments were performed independently at least three times. Source data are provided as a Source Data file. See also Supplementary Fig. 8.

Microscopy
The fluorescence photographs were taken by Olympus BX53 microscope with a DP80 camera. Development statistics were taken by Olympus MVX10 dissecting microscope with a DP80 camera. The confocal images were taken by inverted Zeiss LSM 880/900 confocal microscope system equipped with an alpha Plan-Apochromat 363 oil-immersion objective lens, and processed and analyzed with ZEN imaging software (v.3.4).

Quantification
Animals were randomly selected for fluorescent photography. The size of transgene worms was photographed by the Nomarski microscope and measured by ImageJ software. ImageJ software was used for quantifying fluorescence intensity of indicated animals, which was then normalized with control group.

Statistical analysis
All experiments were performed independently at least three times with similar results. All statistical analyses were preformed using unpaired two-tailed Student's *t*-test, except for Supplementary Fig. 1b which was analyzed by using the Chi-square test. Statistical parameters are presented as mean ± SEM, statistical significance ($P < 0.05$, *, $P < 0.01$, **, $P < 0.001$, ***), and "*n*" (the number of worms counted). The phenotype observations in our experiments were conducted in a blinded manner to genotype.

Reporting summary
Further information on research design is available in the Nature Portfolio Reporting Summary linked to this article.

Data availability
All data in main Manuscript and Supplementary information are listed in the Source data file. All reagents and strains generated by this study are available through request to the corresponding author with a completed Material Transfer Agreement. Source data are provided with this paper.

References

1. Brookes, S. J. H., Spencer, N. J., Costa, M. & Zagorodnyuk, V. P. Extrinsic primary afferent signalling in the gut. *Nat. Rev. Gastro Hepat.* **10**, 286–296 (2013).
2. Chambers, A. P., Sandoval, D. A. & Seeley, R. J. Integration of satiety signals by the central nervous system. *Curr. Biol.* **23**, R379–R388 (2013).
3. Guerra, A. et al. Relevance and challenges in modeling human gastric and small intestinal digestion. *Trends Biotechnol.* **30**, 591–600 (2012).
4. Qi, B., Kniazeva, M. & Han, M. A vitamin-B2-sensing mechanism that regulates gut protease activity to impact animal's food behavior and growth. *Elife* **6**, e26243 (2017).
5. Geng, S. et al. Gut commensal E. coli outer membrane proteins activate the host food digestive system through neural-immune communication. *Cell Host Microbe.* **30**, 1401–1416.e1408 (2022).
6. Liu, H. & Qi, B. Protocol for investigating the effect of food digestion in C. elegans on development by feeding the inedible bacteria Staphylococcus saprophyticus. *STAR Protoc.* **4**, 101990 (2023).
7. Hao, F., Liu, H. & Qi, B. Bacterial peptidoglycan acts as a digestive signal mediating host adaptation to diverse food resources in C. elegans. *Nat. Commun.* **15**, 3286 (2024).
8. Drougard, A., Fournel, A., Valet, P. & Knauf, C. Impact of hypothalamic reactive oxygen species in the regulation of energy metabolism and food intake. *Front Neurosci.* **9**, 56 (2015).
9. Andrews, Z. B. et al. UCP2 mediates ghrelin's action on NPY/AgRP neurons by lowering free radicals. *Nature* **454**, 846–851 (2008).
10. Vahid, F., Wagener, L., Leners, B. & Bohn, T. Pro- and antioxidant effect of food items and matrices during simulated in vitro digestion. *Foods* **12**, 1719 (2023).
11. Li, X. et al. High-fat diet promotes experimental colitis by inducing oxidative stress in the colon. *Am. J. Physiol.-Gastr L* **317**, G453–G462 (2019).
12. Graves, J. A., Metukuri, M., Scott, D., Rothermund, K. & Prochownik, E. V. Regulation of reactive oxygen species homeostasis by peroxiredoxins and c-Myc. *J. Biol. Chem.* **284**, 6520–6529 (2009).
13. Xia, Q. et al. Peroxiredoxin 2 regulates DAF-16/FOXO mediated mitochondrial remodelling in response to exercise that is disrupted in ageing. *Mol. Metab.* **88**, 102003 (2024).
14. Jia, Q., Young, D. & Sieburth, D. Endogenous hydrogen peroxide positively regulates secretion of a gut-derived peptide in neuroendocrine potentiation of the oxidative stress response in C. elegans. *Elife* **13**, RP97503 (2024).
15. Quintin, S., Aspert, T., Ye, T. & Charvin, G. Distinct mechanisms underlie H2O2 sensing in C. elegans head and tail. *PLoS One* **17**, e0274226 (2022).
16. Bhatla, N. & Horvitz, H. R. Light and hydrogen peroxide inhibit C. elegans feeding through gustatory receptor orthologs and pharyngeal neurons. *Neuron* **85**, 804–818 (2015).
17. Li, G., Gong, J. K., Lei, H. Y., Liu, J. F. & Xu, X. Z. S. Promotion of behavior and neuronal function by reactive oxygen species in. *Nat. Commun.* **7**, 13234 (2016).
18. Shpilka, T. & Haynes, C. M. The mitochondrial UPR: mechanisms, physiological functions and implications in ageing. *Nat. Rev. Mol. Cell Biol.* **19**, 109–120 (2018).
19. Shpilka, T. et al. UPR(mt) scales mitochondrial network expansion with protein synthesis via mitochondrial import in Caenorhabditis elegans. *Nat. Commun.* **12**, 479 (2021).
20. Nargund, A. M., Pellegrino, M. W., Fiorese, C. J., Baker, B. M. & Haynes, C. M. Mitochondrial import efficiency of ATFS-1 regulates mitochondrial UPR activation. *Science* **337**, 587–590 (2012).
21. Haynes, C. M., Petrova, K., Benedetti, C., Yang, Y. & Ron, D. ClpP mediates activation of a mitochondrial unfolded protein response in C-elegans. *Dev. Cell* **13**, 467–480 (2007).
22. Tian, Y. et al. Mitochondrial stress induces chromatin reorganization to promote longevity and UPRmt. *Cell* **165**, 1197–1208 (2016).
23. Zhang, Q. et al. The mitochondrial unfolded protein response is mediated cell-non-autonomously by retromer-dependent Wnt signaling. *Cell* **174**, 870 (2018).

24. Chalasani, S. H. et al. Neuropeptide feedback modifies odor-evoked dynamics in olfactory neurons. *Nat. Neurosci.* **13**, 615–U130 (2010).
25. Lee, H. K., Park, K.-S. & Yoon, K.-h. Mitochondrial calcium uniporter regulates odor learning and memory by controlling neuropeptide release. *bioRxiv* **13**, RP102642 (2023).
26. Speese, S. et al. UNC-31 (CAPS) is required for dense-core vesicle but not synaptic vesicle exocytosis in Caenorhabditis elegans. *J. Neurosci.* **27**, 6150–6162 (2007).
27. Sengupta, L. The belly rules the nose: feeding state-dependent modulation of peripheral chemosensory responses. *Curr. Opin. Neurobiol.* **23**, 68–75 (2013).
28. Conradt, B. & Horvitz, H. R. The protein EGL-1 is required for programmed cell death and interacts with the Bcl-2-like protein CED-9. *Cell* **93**, 519–529 (1998).
29. Beverly, M., Anbil, S. & Sengupta, P. Degeneracy and neuromodulation among thermosensory neurons contribute to robust thermosensory behaviors in. *J. Neurosci.* **31**, 11718–11727 (2011).
30. Dishart, J. G. et al. Olfaction regulates peripheral mitophagy and mitochondrial function. *Sci. Adv.* **10**, eadn0014 (2024).
31. L'Etoile, N. D. & Bargmann, C. I. Olfaction and odor discrimination are mediated by the guanylyl cyclase ODR-1. *Neuron* **25**, 575–586 (2000).
32. Biron, D., Wasserman, S., Thomas, J. H., Samuel, A. D. T. & Sengupta, P. An olfactory neuron responds stochastically to temperature and modulates thermotactic behavior. *P Natl Acad. Sci. USA* **105**, 11002–11007 (2008).
33. De-Souza, E. A., Thompson, M. A. & Taylor, R. C. Olfactory chemosensation extends lifespan through TGF-β signaling and UPR activation. *Nat. Aging* **3**, 938–947 (2023).
34. Oláhová, M. et al. A redox-sensitive peroxiredoxin that is important for longevity has tissue- and stress-specific roles in stress resistance. *Proc. Natl Acad. Sci. USA* **105**, 19839–19844 (2008).
35. Oláhová, M. & Veal, E. A. A peroxiredoxin, PRDX-2, is required for insulin secretion and insulin/IIS-dependent regulation of stress resistance and longevity. *Aging Cell* **14**, 558–568 (2015).
36. Jia, Q. & Sieburth, D. Mitochondrial hydrogen peroxide positively regulates neuropeptide secretion during diet-induced activation of the oxidative stress response. *Nat. Commun.* **12**, 2304 (2021).
37. Durieux, J., Wolff, S. & Dillin, A. The cell-non-autonomous nature of electron transport chain-mediated longevity. *Cell* **144**, 79–91 (2011).
38. Berendzen, K. M. et al. Neuroendocrine coordination of mitochondrial stress signaling and proteostasis. *Cell* **166**, 1553 (2016).
39. Chen, L. T. et al. Neuronal mitochondrial dynamics coordinate systemic mitochondrial morphology and stress response to confer pathogen resistance in C. elegans. *Dev. Cell* **56**, 1770 (2021).
40. Shao, L. W., Niu, R. & Liu, Y. Neuropeptide signals cell non-autonomous mitochondrial unfolded protein response. *Cell Res.* **26**, 1182–1196 (2016).
41. Dickinson, D. J., Ward, J. D., Reiner, D. J. & Goldstein, B. Engineering the genome using Cas9-triggered homologous recombination. *Nat. Methods* **10**, 1028 (2013).
42. Chen, Y., Yang, R., Qi, B. & Shan, Z. Peptidoglycan-Chi3l1 interaction shapes gut microbiota in intestinal mucus layer. *Elife* **13**, RP92994 (2024).
43. Kamath, R. S. et al. Systematic functional analysis of the Caenorhabditis elegans genome using RNAi. *Nature* **421**, 231–237 (2003).
44. Rual, J. F. et al. Toward improving Caenorhabditis elegans phenome mapping with an ORFeome-based RNAi library. *Genome Res.* **14**, 2162–2168 (2004).
45. Nayak, D. et al. Biofilm impeding AgNPs target skin carcinoma by inducing mitochondrial membrane depolarization mediated through ROS production. *Acs Appl Mater. Inter* **8**, 28538–28553 (2016).
46. Xu, S. H. & Chisholm, A. D. C. elegans epidermal wounding induces a mitochondrial ROS burst that promotes wound repair. *Dev. Cell* **31**, 48–60 (2014).

Acknowledgements

We thank the Caenorhabditis Genetics Center (CGC) (funded by NIH P40OD010440) for strains; We thank Dr. Chongling Yang (Yunnan University), Dr. Shangbang Gao (Huazhong University of Science and Technology), Dr. Xiajing Tong (ShanghaiTech University) for sharing strains. This work was supported by the Ministry of Science and Technology of the People's Republic of China (2019YFA0803100, 2019YFA0802100 to B.Q.), the National Natural Science Foundation of China (32071129 to Z.S., 32170794 to B.Q.), Yunnan Provincial Science and Technology Project at Southwest United Graduate School (202302AP370005 to B.Q.), Yunnan Applied Basic Research Projects (202201AT070196 to B.Q.), Science and Technological Talent Cultivation Plan of Yunnan Province (C619300A086 to Z.S., K264202230211 to B.Q.).

Author contributions

Y. L. and Q.L. performed experiments, analyzed data. Y.L., G.T., X.Z., P.C. performed RNAi screen, B.C. performed GO enrichment analysis. Z.S. wrote/modified the manuscript and provided some critical suggestions. B.Q. supervised this study, and wrote the paper with inputs from Y.L. and Q.L.

Competing interests

The authors declare no competing interests.

Additional information

Supplementary information The online version contains supplementary material available at https://doi.org/10.1038/s41467-024-55013-3.

Correspondence and requests for materials should be addressed to Zhao Shan or Bin Qi.

Peer review information *Nature Communications* thanks the anonymous reviewer(s) for their contribution to the peer review of this work. A peer review file is available.